Carbon 182 (2021) 175–184

Contents lists available at ScienceDirect

Carbon

journal homepage: www.elsevier.com/locate/carbon

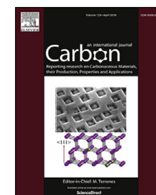

Atomic-scale and damage-free polishing of single crystal diamond enhanced by atmospheric pressure inductively coupled plasma

Hu Luo [a], Khan Muhammad Ajmal [a], Wang Liu [a], Kazuya Yamamura [b], Hui Deng [a, *]

[a] Department of Mechanical and Energy Engineering, Southern University of Science and Technology, No. 1088, Xueyuan Road, Shenzhen, Guangdong, 518055, China

[b] Department of Precision Engineering, Graduate School of Engineering, Osaka University, 2-1 Yamadaoka, Suita, Osaka, 565-0871, Japan

ARTICLE INFO

Article history:
Received 13 April 2021
Received in revised form
27 May 2021
Accepted 28 May 2021
Available online 3 June 2021

Keywords:
Diamond polishing
Damage-free surface
ICP enhanced polishing
Atomic surface
OH radicals

ABSTRACT

Diamond is an imperative material for fabricating functional components used in ultra-hard cutting tools, infrared optical windows, high-performance heat dissipations, and other fields. However, high surface roughness caused by competitive crystal growth in diamonds is troublesome. Besides, diamond polishing is challenging due to extreme hardness and chemical inertness. This work is focused on highly efficient and damage-free diamond polishing enhanced by atmospheric pressure inductively coupled plasma (ICP) modified silicon plate. A rapid decrease in the surface roughness from S_a 308 nm–0.86 nm over 300 μm^2 in 120 min proclaims ICP enhanced polishing a highly efficient technique. Simultaneously, an atomically smooth, high-quality diamond surface is obtained with a surface roughness of R_a 0.26 nm over 20 μm^2. The polishing mechanism based on the OH* modification of silicon plate and diamond surface, dehydration condensation reaction occurring at the interface of OH* terminated surfaces, and subsequent mechanical shearing of carbon, is proposed. The optical emission spectra of ICP, and XPS of the polished diamond surface endorse the material removal mechanism. The TEM and Raman analysis of the ICP enhanced polished surfaces promote the damage-free removal of the mechanically induced damaged layer. The ICP enhanced polishing with modified silicon plate shows great potential in damage-free atomic processing and a promising future as a commercial diamond polishing technique.

© 2021 Elsevier Ltd. All rights reserved.

1. Introduction

Diamond is one of the most promising materials of the 21st century, owing to excellent chemical-mechanical and optical properties [1–3]. These exceptional properties make diamond an irreplaceable material in modern industrial applications, such as ultra-hard cutting tools, infrared optical windows, high-performance heat dissipations, etc. [4–6]. Furthermore, higher values of electric field breakdown strength (10 MV/cm), bandgap (5.5 eV), and thermal conductivity (2000 W/MK) of single crystal diamond (SCD) are ideal for fabricating high-performance semiconductor electronic components [7,8]. Unfortunately, the high surface roughness of natural and synthetic diamonds is troublesome for applications seeking highly smooth diamond surfaces. For example, high roughness can spoil the Q-factor in Micro-Electro-Mechanical Systems (MEMS), create dispersion in surface acoustic wave (SAW) applications, and cause light diffusion in optical applications [9]. Therefore, an efficient and high-quality diamond polishing technology is indispensable. However, it is rather challenging to polish diamonds because of the extreme hardness and chemical inertness.

The mechanical polishing of diamonds is the most widely used method that employs a diamond grit metal plate called Scaife. Initially, the diamond polishing predominantly focused on improving the Scaife wheel performance for material removal, which depends on the mechanical abrasion between the diamond sample pressed against a rotating cast iron wheel [10–12]. Kubota et al. [13] developed an enhanced diamond grit charging method for ultra-smooth mechanical polishing of diamonds. Apart from the typical Scaife method, various techniques have been developed to improve mechanical polishing performance. Ralchenko et al. [14] introduced ultrasonic vibration enhanced mechanical polishing, reducing the surface roughness from Ra 5 μm–0.5 μm (70 μm × 52 μm) in 5 min. Tang et al. [15] employed a bulk diamond substrate to polish diamond films and obtained a material removal rate (MRR) of 10 μm/h, much higher than the traditional mechanical polishing.

* Corresponding author.
E-mail address: dengh@sustech.edu.cn (H. Deng).

https://doi.org/10.1016/j.carbon.2021.05.062
0008-6223/© 2021 Elsevier Ltd. All rights reserved.

However, mechanical polishing introduces severe damages to the polished surfaces, such as scratches, cracks, residual stress, and defects [12,16]. Additionally, microcleavage caused by the anisotropic material removal in mechanical polishing strongly depends on the crystal orientation and polishing direction of SCD [17,18].

In recent decades, the combination of mechanical, chemical, and thermal polishing has been extensively used to enhance material removal efficiency and improve polished surface quality. The chemical-mechanical polishing (CMP), also known as thermal oxidation polishing, utilizes mechanical polishing in conjunction with chemicals to improve the surface quality and MRR [19–21]. Yuan et al. [19] systematically investigated the polishing performance of 10 different CMP slurries. They found that the slurry with potassium ferrate (K_2FeO_4) oxidant provides the highest MRR of 0.055 mg/h and lowest surface roughness of Ra 0.187 nm (10 μm × 10 μm). Thomas et al. [21] employed CMP to flatten the nanocrystalline diamond (NCD) films. The surface roughness decreased from Ra 18.3 nm–1.7 nm over 25 μm^2 after 4 h of polishing at an MRR of 16 nm/h. It was established that wet oxidation of the surface, attachment of silica particles, and subsequent removal of carbon atoms were responsible for the material removal. Lu et al. [22] experimentally investigated the SCD polishing performance of the sol-gel polishing tool after the CMP. Results show that nanoscale subsurface damages, including amorphization, dislocation, and lattice distortion, can be observed in the soft direction. Dynamic friction polishing (DFP) [23–26] of diamonds utilizes the heat produced by friction to convert diamond carbon into non-diamond carbon. Subsequently, the non-diamond carbon is removed either mechanically by the rotating metal plate or oxidized to form CO or CO2 and evaporated. These methods combine mechanical and chemical effects to obtain high material removal efficiency and ultra-fine diamond polishing. However, there are several challenges faced by mechanical, chemical, or a combination of chemical-mechanical polishing of diamonds. Due to the abrasive abrasion, the surface damages cannot be avoided [22]. The pollutants induced by the chemicals during CMP result in non-diamond contamination on the polished diamond surface [9,21]. Although the CMP employing soft silica abrasives can obtain an ultra-smooth diamond surface, the corresponding MRR is far from satisfactory. High polishing load and fast sliding speed in DFP induce cracks and damages the diamond surface [27,28]. Besides, due to melting at high temperatures, the metal plate adheres a metallic layer to the polished diamond surface, which is very difficult to remove [29].

State of the art OH radicals (OH*) assisted diamond polishing has attracted increasing attention in recent years. Kubota et al. [30,31] introduced abrasive free SCD polishing, employing a rotating iron plate immersed in hydrogen peroxide (H_2O_2). According to the results, the surface roughness was improved from Ra 1.87 nm–0.13 nm (72 μm × 72 μm) after 10 h of polishing. Watanabe et al. [32] utilized ultraviolet irradiation induced photochemical reactions to produce OH* for the ultraprecision diamond polishing. The obtained MRR was about 0.5 μm/h, much higher than polishing without UV irradiation. Similarly, Kubota et al. [33] proposed vacuum-ultraviolet (VUV) irradiation assisted SCD planarization and found that the MRR of VUV assisted polishing is about 7 times that of conventional polishing. Yamamura et al. [34,35] developed plasma-assisted polishing (PAP) of diamonds and obtained a damage-free surface with a surface roughness of Ra 0.46 nm (5 μm × 5 μm). The MRR of PAP was improved from 2.17 μm/h to 13.3 μm/h by adding oxygen (O_2) in the plasma feed gas. The atomic-scale smoothening and damage-free finishing of diamonds based on the chemical reaction between OH* and the diamond surface is a major advantage of modern techniques over conventional methods that utilize abrasives. However, commercial applications of current techniques require improved polishing efficiency. Although the PAP is a promising technique with MRR up to 2.17 μm/h, the complex machining facilities and vacuum processing conditions are challenging for industrial application.

In this paper, atmospheric pressure inductively coupled plasma (ICP) enhanced PAP of SCD is proposed based on the ICP generated OH* modified monocrystalline silicon polishing plate, hereafter written as ICP enhanced PAP. The ICP enhanced PAP improves machining efficiency and polished surface quality. It is important to mention that no abrasives are used for polishing, and the chemical reactions between the modified monocrystalline silicon plate and diamond surface are responsible for material removal from the diamond surface. The material removal mechanism is supported by the optical emission spectroscopy (OES) of the ICP jet, and the X-ray photoelectron spectroscopy (XPS) of the polished diamond surface. The polishing efficiency is determined by the rapidly decreasing surface roughness from Sa 308 nm–0.86 nm within 120 min. The damage-free ICP enhanced PAP of diamonds is proven by the Raman spectroscopy and high magnification transmission electron microscopy (TEM).

2. Experimental details

2.1. Principle and experimental setup of ICP enhanced diamond polishing

The principle of ICP enhanced PAP of SCD is shown in Fig. 1. The ICP jet and the diamond sample are both aligned vertically on the same concentric circle at the polishing disc to ensure that the diamond surface is in contact with the modified plate region, as shown in Fig. 1a. A holder fixes the diamond sample, and a load adjusting system controls the vertically applied force. The material removal is realized when the diamond surface is pressed against the ICP modified silicon plate rotating about its axis. ICP plasma generates abundance of OH* that adhere and activate the silicon plate, as shown in Fig. 1b. These OH* are transferred to the diamond surface once it is engaged with the modified silicon surface. Besides, the high-temperature ICP rapidly increases the polishing interface temperature to hundreds of degrees, providing sufficient activation energy for chemical bond recombination. When diamond and silicon surfaces contact each other at sufficiently high temperatures, OH* undergo dehydration condensation reaction at the polishing interface, and form new chemical bonds, such as *C*–C, *C*–O, Si–O, Si–Si, and *C*–O–Si. Among them, the *C*–C bond has the lowest binding energy [21]. The *C*–C bonds break due to frictional shear between the two surfaces, and the carbon atoms are removed. The protrusions on the diamond surface are more likely to capture OH* and undergo preferential chemical reaction than the substrate. Simultaneously, the carbon atom bonding at protrusions become weak and easily removed either chemically or mechanically. This is how a rough diamond surface is polished by ICP enhanced PAP.

The ICP enhanced PAP experimental setup consists of three-axis numerical control (NC) platform, rotation table, plasma generator, and workpiece motion controller, as shown in Fig. 1c. The rotation of the workpiece shaft holding the diamond substrate is controlled by a small motor, while the NC platform monitors the position of the diamond substrate. The polishing load is adjusted by the counterweight installed on the workpiece motion platform.

2.2. Materials and characterization

The polishing plate should have good thermal conductivity for the ultra-high temperature of generated ICP plasma. According to Ref. [34], the hardness of the polishing plate is significant to obtain

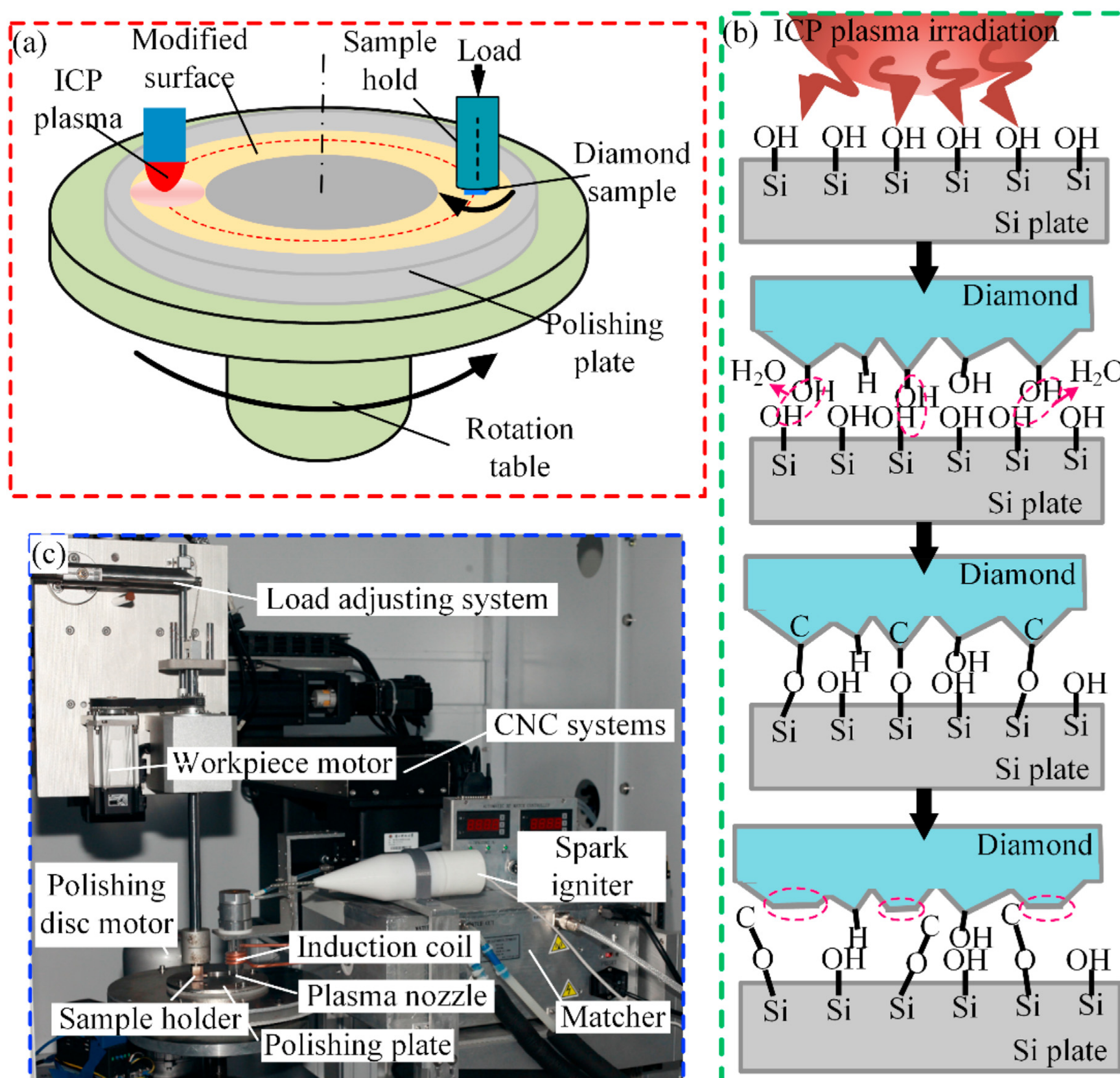

Fig. 1. Experimental setup of ICP enhanced PAP of diamonds: (a) polishing principle, (b) material removal mechanism, and (c) experimental apparatus. (A colour version of this figure can be viewed online.)

a damage-free diamond surface. Silicon is one of the best thermal conductors and the second hardest among the SiO_2, Al_2O_3, and silicon. Therefore, silicon is chosen as the polishing plate material because of the excellent balance between thermal conductivity and hardness. A CMP processed monocrystalline silicon wafer with a diameter of $\phi100 \pm 0.3$ mm and thickness of 3 ± 0.025 mm, taken from Single Side Polish Wafers Co., Ltd. (China), was used as a polishing plate. The <100> SCDs having $4 \times 4 \times 2$ mm^3 dimensions, purchased from Ningbo Crysdirm Industrial Technology Co., Ltd. (China), were used in experiments. Before ICP enhanced PAP, rough diamond surfaces were prepared by ICP etching. In etching experiments, CF_4 was used as a plasma feed gas, and the surface roughness of SCD after etching was increased to hundreds of nanometers. The mechanically polished diamonds were used in the subsurface damage experiments. During polishing, argon (Ar) gas was used as ICP plasma feed, while H_2O_2 was mixed in the feed gas to improve OH* number density in the discharge.

The weight of the diamond samples before and after polishing was measured by an electronic balance (Mettler Toledo XSR105, Switzerland) with a resolution of 0.01 mg. The MRR can be calculated by the following equation:

$$\mathrm{MRR} = \frac{10^3 \times \Delta m}{\rho S t} \tag{1}$$

where Δm (mg) is the mass loss during polishing, ρ (3.45 g/cm^3) is the density, S (16 mm^2) is the surface contact area, t (min) is the processing time, and MRR (μm/h) is the corresponding removal rate of SCD.

The polishing plate temperature was determined by an infrared thermal camera (FLIR T660, USA), with the emissivity calibration performed by the contact thermometer method. At first, the infrared camera was employed to record the entire polishing process. Then, the FLIR tools software was used to analyze and acquire the detailed temperature of the polishing plate. The surface roughness was measured by white light interferometer (Taylor Hobson CCI HD, UK) and atomic force microscope (AFM, Bruker Dimension edge, USA). The average surface roughness was measured from three random points on the same surface. The OES was recorded by a modular spectrometer (Ocean Optics Products

Co., Ltd. USA). The XPS was recorded by PHI 5000 VersaProbe III spectrometer using a monochromatic Al K_α X-ray source, with X-ray generated at 100 μm, 25 W, 15 kV. During data acquisition, broad and narrow survey scans of pertinent peaks were obtained at pass energies of 280 eV and 69 eV, respectively. The sectional TEM samples were prepared by a focused ion beam (FEI Helios Nanolab 600i, USA). The prepared samples were observed on a transmission electron microscope (JEM-3200FS, Japan), operated at 300 kV. Raman spectra were acquired by a laser confocal Raman spectrometer (Horiba LabRAM HR Evolution, France) with a 785 nm laser source. The diamond surfaces were ultrasonically cleaned with absolute ethanol and deionized water before XPS measurements and FIB sample preparation.

2.3. Design of experiments

The material removal during polishing strongly depends on the OH* concentration in the discharge. The OH* concentration in the discharge depends on the reactive gas flow rate and ICP power input. In the first set of experiments, reactive gas flow rate and ICP power input were optimized to achieve a maximum possible concentration of OH*. The reactive gas flow rate varied from 2 to 6 sccm at an increment of 1 sccm. The ICP power input was swept from 300 to 700 W with 100 W increment. Simultaneously, the maximum OH* concentration in the discharge was identified by comparing the OES.

In the second set of experiments, the effect of OH* concentration on MRR was investigated. The OH* concentration was adjusted by increasing Ar gas flow rate from 2 to 5 sccm while keeping the rest of the experimental parameters constant, such as a polishing load of 1.2 ± 0.1 N, polishing plate rotation speed 300 rpm, workpiece speed 0 rpm, ICP power input 500 W, and polishing time 1 h. Similarly, the effect of OH* concentration was also investigated by performing a control group under the same experimental conditions, except the reactive feed gas passing through H_2O_2.

In the third set of experiments, a highly rough diamond was polished by ICP enhanced PAP at a load of 1 ± 0.1 N, polishing plate rotation speed 300 rpm, workpiece rotation speed 30 rpm, and ICP power 500 W. The surface roughness during polishing was recorded every 20 min until the roughness did not improve further. The damage-free nature of ICP enhanced PAP was investigated by characterizing as-received and polished diamonds by Raman and TEM. The experimental conditions were set the same as the polishing performance experiments with 1 h of polishing time.

3. Results and discussions

3.1. Material removal mechanism

Although OH* play a leading role in material removal during diamond polishing [21], the lack of evidence makes it hard to believe the hypothesis. Besides, OES can identify OH* in the ICP, but it is hard to determine its discharge concentration. Therefore, the OH* concentration is determined from the intensity ratio (I_{OH*}/I_{Ar}) variation under different conditions [36].

The OES of ICP operated at 500 W power input and the Ar flow rate of 3 sccm with/without H_2O_2 vapor is shown in Fig. 2a. The species observed in the ICP spectra are in excellent agreement with previous studies [36,37]. Ar emission lines mainly dominate the optical emission between 400 nm and 820 nm. However, the hydrogen emission lines at 434 nm, 656 nm, and 486 nm were observed when the reactive Ar gas was mixed with the H_2O_2. The electron-impact excitation ($e^- + H_2O\ OH^* + H^* + e^-$) is responsible for OH* band emission at 306–312 nm, as shown in the inset of Fig. 2a [38]. Similarly, the OH* can also be obtained from the H_2O_2 vapor mixed with the feed gas. The electron impact dissociation of oxygen molecules (O_2) from the air and H_2O_2 results in the atomic O emission at 777 nm and 844 nm.

The effect of reactive gas flow rate and ICP power input on OH* concentration is shown in Fig. 2b. The OH* concentration increases with the flow rate and keeps decreasing with the rising ICP power input unless the flow rate effect becomes insignificant at 700 W. According to the feed gas system, Ar is mixed with the H_2O_2 vapor in an enclosed vessel and then supplied to the ICP. Therefore, a higher flow rate increases electron-impact collisions with the H_2O_2 vapor and produces higher OH* concentration. The situation becomes complicated when the discharge temperature rises rapidly with the ICP power input. Accordingly, the flow rate of cooling Ar gas is increased during processing, which mixes cooling gas in the discharge and increases Ar concentration. However, the OH* concentration only depend on the reactive gas flow rate. So, the ratio I_{OH*}/I_{Ar} decreases with the increasing ICP power input. The polishing plate temperature increases with increasing ICP power input, as shown in Fig. 2c, which is due to the electron-impact energy transfer to the feed gas species. The polishing plate temperature recorded at 500 W power input is 262.3 C°, appropriate for activating the chemical bonds and promoting the chemical reaction between the modified silicon plate and diamond surface.

There is a paradox in selecting the ICP power input. The higher input power would increase the polishing plate temperature and accelerate the polishing process. Besides, it is the OH* radical that plays a key role in material removal during the PAP process. Therefore, making OH* species concentration as high as possible is necessary for high removal efficiency. As evident from Fig. 2b, the highest OH* concentration is produced at 400 W and is appropriate for the polishing process. In practice, the ICP discharge appears filamentary at low power input and high gas flow rate, resulting in frequent failure. However, the ICP discharge becomes stable when the power input exceeds 500 W and the gas flow rate is less than 5 sccm. Therefore, ICP is operated at 500 W power input and 5 sccm gas flow rate in subsequent experiments.

Fig. 2d shows the effect of reactive gas flow rate on MRR. The MRR increases from 0.79 μm/h to 1.5 μm/h with the H_2O_2 vapor mixed Ar gas flow rate increasing from 2 sccm to 5 sccm. An insignificant change in the MRR is observed with the increasing reactive Ar flow rate without H_2O_2 vapor mixing. However, the MRR is almost 0 when without ICP. This is because there is no chemical reaction involved in material removal during polishing process without ICP plasma modification. And the abrasive-free and small polishing pressure lead to the absence of mechanical shear effect during polishing. As discussed, the OH* concentration and the chemical reaction at the polishing plate and diamond surface interface increase when the H_2O_2 vapor mixed reactive gas flow rate increases. Therefore, the corresponding MRR also increases.

XPS has been widely used to analyze the chemical bond evolution during diamond polishing [9,21]. Similarly, chemical bond evolution at the diamond surface during ICP enhanced PAP is analyzed by XPS, as shown in Fig. 3. The characters of O1s (≈532 eV), C1s (≈285 eV), and Si2p (≈102 eV) are observed in the spectra of the polished diamond surface, and the major photoelectron and Auger peaks are marked by blue arrows, as shown in Fig. 3a. The polishing introduced non-diamond contamination (e.g., Si) on the polished surfaces. However, this level of contamination is acceptable in previously discussed applications. The traditional CMP also introduces such contaminants, but it does not hinder its application in MEMS. Besides, these pollutants are easily cleaned by hydrofluoric acid or plasma exposure.

The C1s peak is appropriate for revealing the evolution of diamond surface chemistry. The deconvolution of C1s peak into four

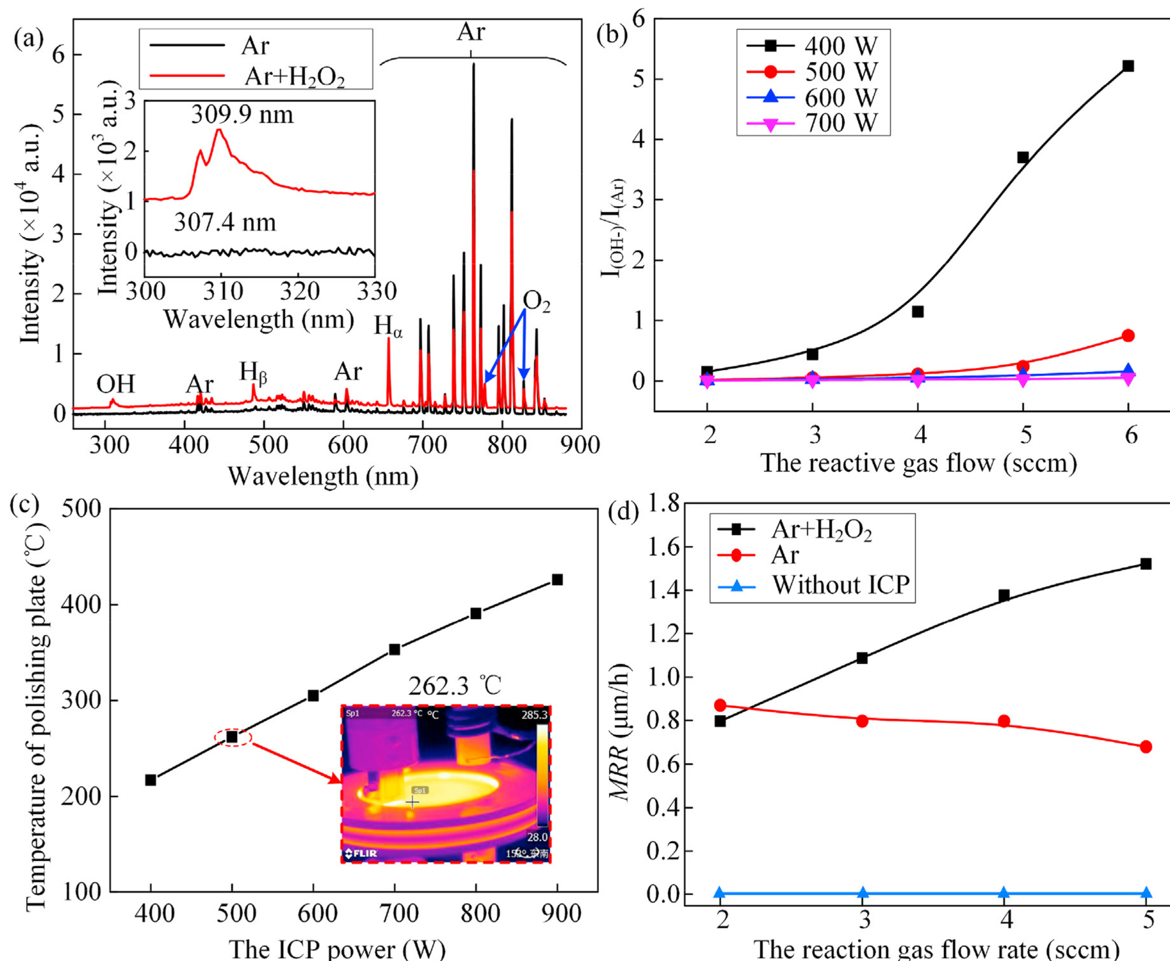

Fig. 2. Properties of the polishing tool: (a) emission spectra of ICP, (b) effect of reactive gas flow rate and ICP power input on the OH* concentration, (c) dependence of polishing plate temperature on the ICP power input, and (d) the effect of reactive gas flow rate on MRR. (A colour version of this figure can be viewed online.)

peaks with binding energies (BE) 284.5 eV, 285.0 eV, and 285.8 eV present different chemical environments, as shown in Fig. 3b. The dominant peaks at 284.5 eV and 285.0 eV correspond to non-diamond (sp^2) and diamond (sp^3) carbon, respectively [39,40]. An additional peak at 285.8 eV belonging to C–O–Si [41,42]. The chemical reaction between OH terminated silicon plate and diamond surface forms C–O–Si bonds. The carboxyl peak (*C*–OH, 288.5 eV) is detected at the highest BE [43]. The ICP generated OH* binds with the breaking chemical bonds and form OH terminated surface that is why a carboxyl peak is observed on the diamond surface. As discussed, two different *C*–C bondings, i.e., the dominant phase (sp^3) and the auxiliary phase (sp^2), are observed on the polished diamond surface. As a first thought, the machining related damages might form the auxiliary phase sp^2. However, breaking the sp^3 structure at a very low polishing load and disordering it without abrasives is impossible. Besides, the TEM images (Fig. 6f) indicate no damage to the surface after polishing. Therefore, it is reasonable to assume that the sp^2 phase is formed due to improper chemical vapor deposition (CVD) conditions during diamond growth.

The detailed O1s spectra fitted with multiple peaks with BE 531.0 eV, 532.2 eV, and 533.3 eV can be seen in Fig. 3c. Major peaks at 532.2 eV and 533.3 eV belong to C–O–Si and carboxyl (*C*–OH) bonds, respectively. The BE peak at 531.0 eV potentially refers to Si–O bonding [44,45]. The detailed Si2p spectra with three major peaks at BE of 99.9 eV, 102.3 eV, and 103.7 eV are shown in Fig. 3d. According to the literature, the highest and lowest BE belong to Si–O (103.7 eV) and Si–Si (99.9 eV) bonds [46]. The remaining peak at 102.3 eV is Si–O–C, which is consistent with the detailed spectra in C1s and O1s [41]. The Si–Si and Si–O peaks belong to the debris stripped from the silicon plate. The emission spectra in Fig. 2a describe the presence of atomic oxygen in the ICP, therefore the silicon surface can be oxidized due to ICP exposure. Besides, diamond is harder than silicon, and the diamond protrusions act as grits and strip off the modified silicon plate when two surfaces are engaged. Consequently, the debris adhere to the diamond, and Si–Si and Si–O bonds can be detected on the polished diamond surface.

Up to now, it has been well established that the desired OH* concentration in the ICP chemistry can be obtained by manipulating the flow rate of H_2O_2 mixed Ar gas and the power input. Besides, OH* actively participate in the material removal from the polished diamond surface. The *C*–OH bonds on the diamond surface confirm the OH* attachment to the silicon plate and subsequent transfer to the diamond surface. It is strong evidence of the OH* termination of silicon plate and the diamond surface, which provide the interface for further chemical reactions. Finally, the C–O–Si bonds prove the allowance of the proposed material removal mechanism in ICP enhanced PAP.

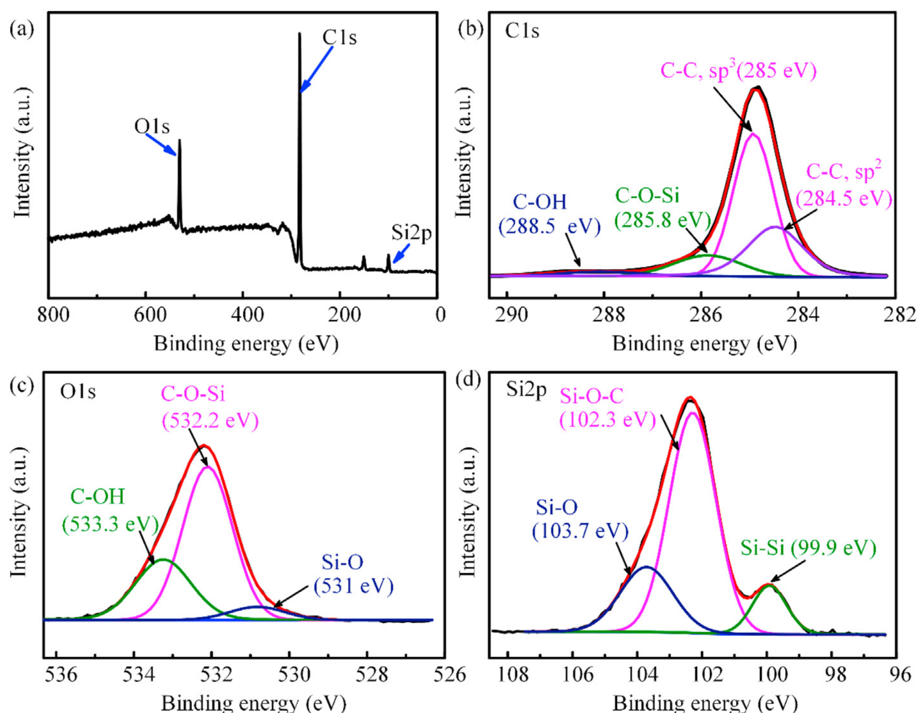

Fig. 3. XPS of the polished diamond surface: (a) main photoelectron and Auger signals, and deconvolution of (b) C1s, (c) O1s, and (d) Si2p. (A colour version of this figure can be viewed online.)

3.2. Polishing efficiency

The ICP enhanced PAP efficiency was evaluated by polishing a rough diamond surface, as shown in Fig. 4. The S_a roughness rapidly reduced from hundreds to tens of nanometers in the first 20 min of ICP enhanced PAP of the diamond surface and became stable at 0.86 nm after 120 min of polishing, as seen from Fig. 4a. Fig. 4b–e shows the micro-topographies at different polishing times. The initial surface is very rough due to micron-scaled peaks and valleys introduced by ICP etching. After 40 min of polishing, the rough peaks are removed, and the S_a roughness is reduced to 30.5 nm. However, some deep valleys and mechanically induced scratches are visible on the polished surface. After 80 min of polishing, all the structures either caused by mechanical polishing (subsurface damages) or ICP etching (etched holes) are removed, and the S_a roughness is reduced to 1.12 nm. Finally, an ultra-smooth polished diamond surface with an atomic scale S_a roughness of 0.86 nm is obtained after 120 min of ICP enhanced PAP.

As discussed, the S_a roughness drops very quickly at the early stage (0–40 min) and then becomes adequately slow at the later

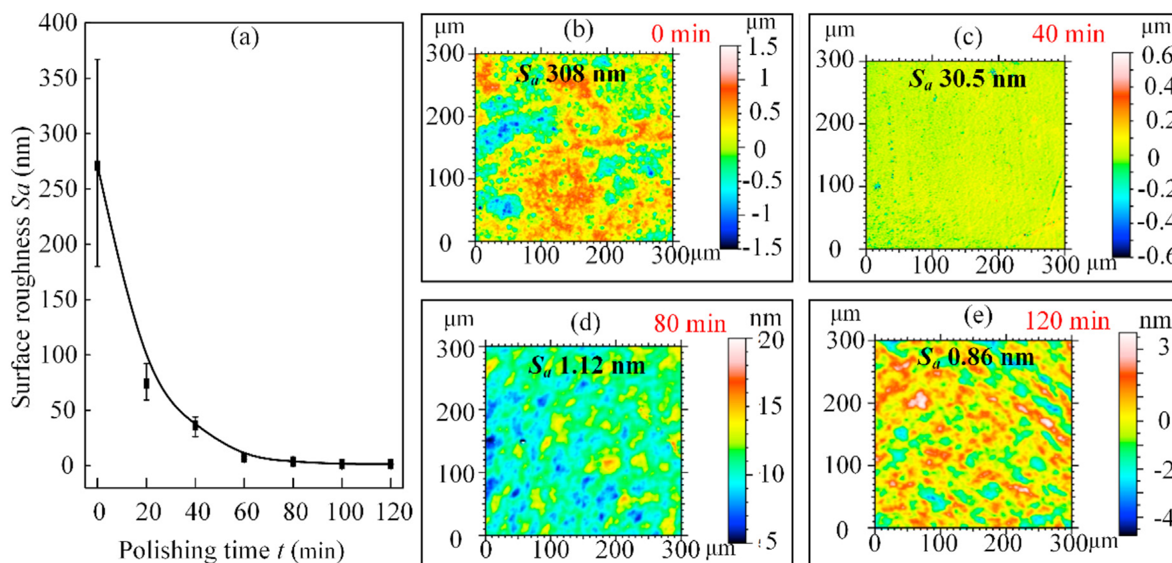

Fig. 4. (a) Surface roughness changes with polishing time, the 2 d micro-topography images with different polishing times: (b) 0 min, (c) 40 min, (d) 80 min, and (e) 120 min. (A colour version of this figure can be viewed online.)

stage (40–120 min) of ICP enhanced PAP. A rapid decrease in S_a roughness at the early stage is attributed to the preferential removal of protrusions. The OH* from the modified polishing plate preferentially attach to the protrusions and initiate chemical reactions, resulting in the fast removal of peaks from the diamond surface. It is consistent with the proposed material removal mechanism. Furthermore, the actual contact area at the polishing interface gradually increases with the removing protrusions, leading to a decrease in contact pressure under the same polishing load. As a result, the mechanical shear between the diamond and the polishing plate decreases, and so does the material removal efficiency. Therefore, the surface roughness rapidly decreases at the early stage and becomes adequately slow at the later stage of ICP enhanced PAP. In general, the polishing efficiency of ICP enhanced PAP is better than previous studies reporting several nanometers to sub-nanometer improvement in the surface roughness after hours of polishing [21,31,32,34]. Particularly, the average polishing stress used in this study is about ~62.5 kPa, which is similar to 52.6 kPa employed the in traditional PAP process [34]. Not to mention the DFP [26], the best obtained S_a roughness is tens of nanometers despite higher processing efficiency.

3.3. Survey on the polishing damages

A mechanically polished diamond surface is used to evaluate the polishing damage of ICP enhanced PAP. The AFM images of the diamond surface before and after polishing are shown in Fig. 5. The mechanically polished surface contains severe scratches mainly caused by abrasive plowing, as shown in Fig. 5a. Besides, after 60 min of ICP enhanced PAP, a damage-free surface with roughness reduced from R_a 1.35 nm–0.26 nm is obtained, as shown in Fig. 5b. According to the A-A section profile shown in Fig. 5b, the abrasive induced scratches are nearly 4 nm in height and depth, as seen from Fig. 5c. The ICP enhanced PAP flattened these mechanically induced scratches below 1 nm, as described by the section profile in Fig. 5d. Thus ICP enhanced PAP fabricated a damage-free diamond surface without using any abrasives, which is its primary benefit over conventional diamond polishing methods. Whereas the material removal in ICP enhanced PAP mainly depends on the chemical reaction between the diamond surface and the modified polishing plate. Therefore minimal polishing load is applied to generate the necessary mechanical shear at the polishing interface to wipe the chemical bonding. Ultimately, no irregularity or damage is induced on the diamond surface. It should be note that the material removal anisotropy reported in Ref. [16] has not been found in our experiments. As shown in Fig. 5e, the section heights obtained from different directions are scaled in ± 2 nm and show little direction dependence. As discussed before, it is the chemical reaction not the mechanical abrasion caused the material removal so that the material removal anisotropy can be avoided.

Fig. 6 shows the cross-sectional TEM images of the diamond surface before and after polishing, further verifying the damage-free nature of ICP enhanced PAP. For a better comparison, the cross-sectional TEM images of the ICP enhanced PAP and mechanically polished diamond surfaces are acquired in the same <110> crystal orientation, as shown in Fig. 6a and d, respectively. The mechanically polished surface has a prominent amorphous layer at the interface between the protective Pt film and the diamond surface, which is induced by the abrasive plowing. The amorphous layer is nearly 3.9 nm thick, as evident from the high-resolution TEM image in Fig. 6c. Many dislocations are observed at the interface between the amorphous layer and the diamond surface, as caused by the abrasive induced distortion of the diamond lattice. Unlike mechanical polishing, ICP enhanced PAP of the diamond surface is free of subsurface damages and irregularities. The amorphous layer free interface shown in Fig. 6f is convincing

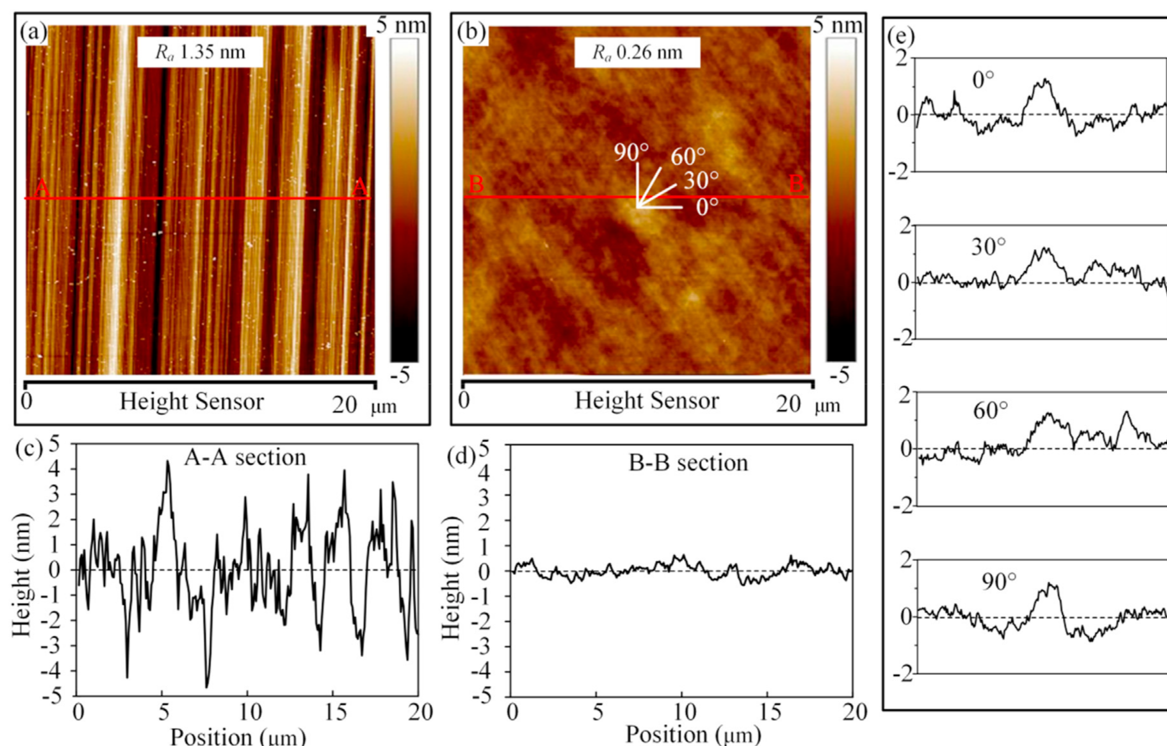

Fig. 5. The AFM images of the diamond surface before and after polishing: (a) initial mechanically polished surface, (b) ICP enhanced polished surface, section profile of (c) A-A, and (d) B–B, (e) section profile at different angles from coordinate shown in Fig. 5(b). (A colour version of this figure can be viewed online.)

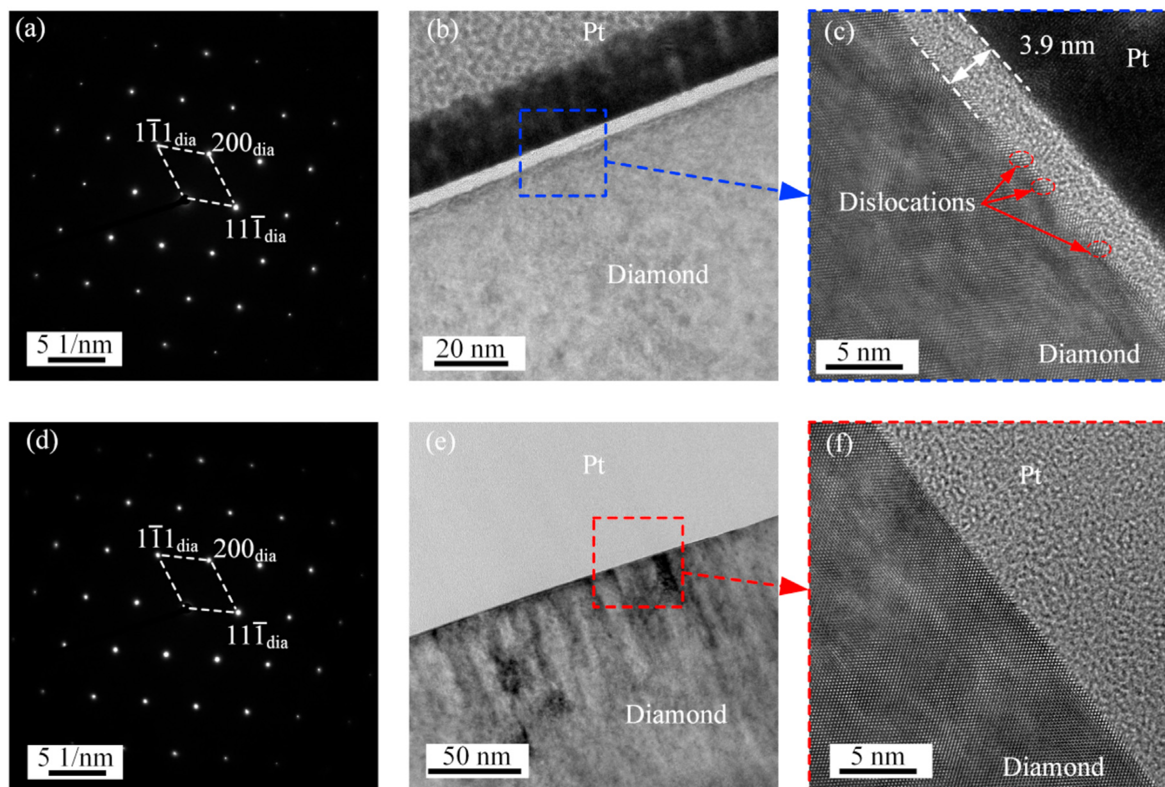

Fig. 6. Subsurface investigation by high-resolution TEM: (a–c) TEM images of the mechanically polished diamond surface obtained at different resolutions: (a) selected area electron diffraction pattern, (b) low, and (c) high magnifications; (d–f) TEM images of ICP enhanced PAP diamond surface obtained at different resolutions: (d) selected area electron diffraction pattern, (e) low, and (f) high magnifications. (A colour version of this figure can be viewed online.)

evidence of the damage-free ICP enhanced PAP of the diamond. The diamond surface remains nearly a perfect lattice with an orderly arrangement of carbon atoms. No apparent dislocations are observed in the atomic layer close to the Pt-diamond interface, indicating individual carbon atom removal rather than the bulk. Therefore, the damage-free processing of diamonds is accomplished owing to the atomic removal mechanism of ICP enhanced PAP.

Raman spectroscopy is another powerful technique to characterize damages and defects in carbon-related materials, particularly diamonds, due to its excellent sensitivity [47]. Fig. 7 shows the Raman spectra of the ICP enhanced PAP and mechanically polished diamond surfaces. The phonon peaks are located at 1332.4 cm^{-1} and 1425.5 cm^{-1}. The sharp phonon peak at 1332.4 cm^{-1} represents the diamond carbon spectrum [34]. A weak and broad intensity peak at 1425.5 cm^{-1} is attributed to non-diamond carbon induced by the mechanical shear [48]. According to Ferrari et al. [49], the upper limit of the diamond band spectra is below 1350 cm^{-1}. Theoretically, the sp^3 bonding can only provide modes up to 1350 cm^{-1}. Typically, the observed Raman spectra of the diamond are located around 1332.4 cm^{-1} because ideal sp^3 crystallization is not possible. The intensity peak of pure sp^2 (G band) corresponding to graphite is located at 1580 cm^{-1}. So, the amorphous carbon (a-C) band spectra are located between 1332.4 cm^{-1} and 1580 cm^{-1}, including different carbon bondings, such as sp^3, sp^2, and even sp^1 phases in a-C. The abrasive action on the diamond surface distorts the sp^3 lattice structure and generates a combination of disordered sp^3 and sp^2 on the mechanically polished surface. Therefore, it is concluded that a peak at 1425.5 cm^{-1} represents the mechanical polishing related defects.

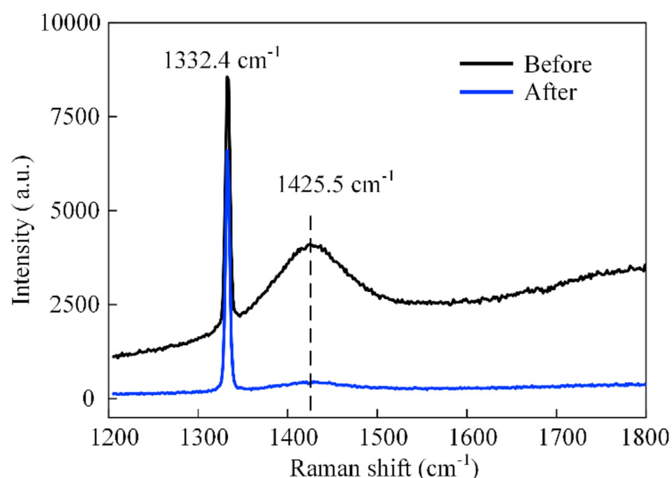

Fig. 7. Raman spectrums before and after ICP enhanced PAP of the diamond. (A colour version of this figure can be viewed online.)

Peak intensity at 1425.5 cm^{-1} became insignificant after ICP enhanced PAP of the mechanically polished diamond. It is believed that the mechanically induced amorphous layer is removed by the ICP enhanced PAP without producing new damages, which agrees well with the AFM and TEM results. The insignificant peak intensity at 1425.5 cm^{-1} after ICP enhanced PAP does not belong to the processing induced damages. Instead, it is caused by the crystal lattice amorphization during diamond growth. The detection of sp^2 phase in XPS results (Fig. 3b), and the absence of dislocations in high-resolution TEM images (Fig. 5f) also advocate the same conclusion.

4. Conclusions

An abrasive-free diamond polishing technique enhanced by the atmospheric ICP modified monocrystalline silicon plate is developed in this work. The following conclusions are derived from the experimental results:

1. According to the proposed polishing mechanism of ICP enhanced PAP, the ICP generated OH* modifies the silicon plate, which in turn facilitates the OH* attachment to the diamond surface. Afterward, a chemical reaction at the interface of two OH terminated surfaces generates weak *C*—Si—O bonds that are easily removed due to the mechanical shear of the polishing plate. The proposed material removal mechanism is extensively supported by the ICP discharge emission spectra containing OH* and the XPS results that confirm the OH* attachment to the diamond surface.
2. The ICP enhanced PAP is a highly efficient diamond polishing technique demonstrated by the rapid decrease in the S_a roughness from 308 nm to 0.86 nm within 120 min polishing. Atomically smooth diamond surface with R_a roughness of 0.26 nm over 25 μm^2 was achieved by the ICP enhanced PAP.
3. The diamond surface after ICP enhanced PAP shows a perfect lattice structure without any dislocations under high-resolution TEM. The Raman spectra indicate that the damage layer induced by mechanical polishing is removed by the ICP enhanced PAP.

In summary, the ICP enhanced PAP is a potential diamond polishing technique that can provide high material removal efficiency and atomically smooth damage-free diamond surfaces simultaneously.

CRediT authorship contribution statement

Hu Luo: Data curation, Formal analysis, Writing — original draft. **Khan Muhammad Ajmal:** Writing — review & editing. **Wang Liu:** Data curation, Methodology. **Kazuya Yamamura:** Methodology, Writing — review & editing. **Hui Deng:** Conceptualization, Supervision, Writing — review & editing.

Declaration of competing interest

The authors declare that they have no known competing financial interests or personal relationships that could have appeared to influence the work reported in this paper.

Acknowledgments

The authors received financial support for this work from the Guangdong Basic and Applied Basic Research Foundation (2019A1515111133), the National Natural Science Foundation of China (No. 52035009, 52005243). The authors acknowledge the assistance of SUSTech Core Research Facilities.

References

[1] N. Yang, S. Yu, J.V. MacPherson, Y. Einaga, H. Zhao, G. Zhao, et al., Conductive diamond: synthesis, properties, and electrochemical applications, Chem. Soc. Rev. 48 (2019) 157–204.
[2] G. Shu, B. Dai, V.G. Ralchenko, A.P. Bolshakov, A.A. Khomich, E.E. Ashkinazi, et al., Growth of three-dimensional diamond mosaics by microwave plasma-assisted chemical vapor deposition, CrystEngComm 20 (2018) 198–203.
[3] J. Heupel, N. Felgen, R. Merz, M. Kopnarski, J.P. Reithmaier, C. Popov, Development of a planarization process for the fabrication of nanocrystalline diamond based photonic structures, Phys. Status Solidi Appl. Mater. Sci. 216 (2019) 1–8.
[4] M.L. Hicks, A.C. Pakpour-Tabrizi, R.B. Jackman, Polishing, preparation and patterning of diamond for device applications, Diam. Relat. Mater. 97 (2019) 107424.
[5] W.J. Zong, K. Cheng, D. Li, T. Sun, Y.C. Liang, The ultimate sharpness of single-crystal diamond cutting tools-Part I: theoretical analyses and predictions, Int. J. Mach. Tool Manufact. 47 (2007) 852–863.
[6] Y.Q. Chen, L.C. Zhang, Polishing of Diamond Materials, Mechanisms, Modeling and Implementation, 1th edn., Springer-Verlag, London, 2013, pp. 25–30.
[7] C.J.H. Wort, R.S. Balmer, Diamond as an electronic material, Mater. Today 11 (2008) 22–28.
[8] C. Dang, J.P. Chou, B. Dai, C.T. Chou, Y. Yang, R. Fan, et al., Achieving large uniform tensile elasticity in microfabricated diamond, Science 371 (2021) 76–78.
[9] S. Mandal, E.L.H. Thomas, L. Gines, D. Morgan, J. Green, E.B. Brousseau, et al., Redox agent enhanced chemical mechanical polishing of thin film diamond, Carbon 130 (2018) 25–30.
[10] J. Wilks, Experiments on polishing of diamond, Nature 243 (1973) 15–18.
[11] M.P. Hitchiner, E.M. Wilks, J. Wilks, The polishing of diamond and diamond composite materials, Wear 94 (1984) 103–120.
[12] T. Jin, M. Ma, B. Li, Y. Gao, Q. Zhao, Z. Zhao, et al., Mechanical polishing of ultrahard nanotwinned diamond via transition into hard sp2-sp3 amorphous carbon, Carbon 161 (2020) 1–6.
[13] A. Kubota, S. Nagae, S. Motoyama, High-precision mechanical polishing method for diamond substrate using micron-sized diamond abrasive grains, Diam. Relat. Mater. 101 (2020) 107644.
[14] V.G. Ralchenko, E.E. Ashkihazi, E.V. Zavedeev, A.A. Khomich, A.P. Bolshakov, S.G. Ryzhkov, et al., High-rate ultrasonic polishing of polycrystalline diamond films, Diam. Relat. Mater. 66 (2016) 171–176.
[15] C.J. Tang, A.J. Neves, A.J.S. Fernandes, J. Grácio, N. Ali, A new elegant technique for polishing CVD diamond films, Diam. Relat. Mater. 12 (2003) 1411–1416.
[16] W.J. Zong, D. Li, K. Cheng, T. Sun, H.X. Wang, Y.C. Liang, The material removal mechanism in mechanical lapping of diamond cutting tools, Int. J. Mach. Tool Manufact. 45 (2005) 783–788.
[17] L. Pastewka, S. Moser, P. Gumbsch, M. Moseler, Anisotropic mechanical amorphization drives wear in diamond, Nat. Mater. 10 (2011) 34–38.
[18] N. Yang, W.J. Zong, Z.Q. Li, T. Sun, The dependency of diamond lapping surface morphology on crystal orientation, Int. J. Adv. Manuf. Technol. 77 (2015) 1029–1034.
[19] Z. Yuan, Z. Jin, Y. Zhang, Q. Wen, Chemical mechanical polishing slurries for chemically vapor-deposited diamond films, J. Manuf. Sci. Eng. Trans. ASME. 135 (2013) 1–8.
[20] J.M. Werrell, S. Mandal, E.L.H. Thomas, E.B. Brousseau, R. Lewis, P. Borri, et al., Effect of slurry composition on the chemical mechanical polishing of thin diamond films, Sci. Technol. Adv. Mater. 18 (2017) 654–663.
[21] E.L.H. Thomas, G.W. Nelson, S. Mandal, J.S. Foord, O.A. Williams, Chemical mechanical polishing of thin film diamond, Carbon N. Y. 68 (2014) 473–479.
[22] Y. Lin, J. Lu, R. Tong, Q. Luo, X.P. Xu, Surface damage of single-crystal diamond (100) processed based on a sol-gel polishing tool, Diam. Relat. Mater. 83 (2018) 46–53.
[23] Y. Chen, L.C. Zhang, J.A. Arsecularatne, C. Montross, Polishing of polycrystalline diamond by the technique of dynamic friction, part 1: prediction of the interface temperature rise, Int. J. Mach. Tool Manufact. 46 (2006) 580–587.
[24] Y. Chen, L.C. Zhang, J.A. Arsecularatne, I. Zarudi, Polishing of polycrystalline diamond by the technique of dynamic friction, part 3: mechanism exploration through debris analysis, Int. J. Mach. Tool Manufact. 47 (2007) 2282–2289.
[25] Y. Chen, L.C. Zhang, J.A. Arsecularatne, Polishing of polycrystalline diamond by the technique of dynamic friction. Part 2: material removal mechanism, Int. J. Mach. Tool Manufact. 47 (2007) 1615–1624.
[26] Y. Chen, L.C. Zhang, Polishing of polycrystalline diamond by the technique of dynamic friction, part 4: establishing the polishing map, Int. J. Mach. Tool Manufact. 49 (2009) 309–314.
[27] Y. Chen, W. Liu, H. Feng, L. Zhang, Failure mechanisms of CVD diamond wafers and thin films during polishing, Mach. Sci. Technol. 19 (2015) 152–173.
[28] F. Tang, Y. Chen, L. Zhang, Analysis of polished polycrystalline diamond using dual beam focused ion beam microscopy, Philos. Mag. A 92 (2012) 1680–1690.
[29] H. Xu, J. Zang, P. Tian, Y. Wang, Y. Yu, J. Lu, et al., Rapid grinding CVD diamond films using corundum grinding wheels containing iron, Int. J. Refract. Metals Hard Mater. 71 (2018) 147–152.
[30] A. Kubota, S. Nagae, M. Touge, Improvement of material removal rate of single-crystal diamond by polishing using H_2O_2 solution, Diam. Relat. Mater. 70 (2016) 39–45.
[31] A. Kubota, S. Motoyama, M. Touge, Development of an Ultra-finishing technique for single-crystal diamond substrate utilizing an iron tool in H2O2 solution, Diam. Relat. Mater. 64 (2016) 177–183.
[32] J. Watanabe, M. Touge, T. Sakamoto, Ultraviolet-irradiated precision polishing of diamond and its related materials, Diam. Relat. Mater. 39 (2013) 14–19.
[33] A. Kubota, T. Takita, Novel planarization method of single-crystal diamond using 172 nm vacuum-ultraviolet light, Precis. Eng. 54 (2018) 269–275.
[34] K. Yamamura, K. Emori, R. Sun, Y. Ohkubo, K. Endo, H. Yamada, et al., Damage-free highly efficient polishing of single-crystal diamond wafer by plasma-assisted polishing, CIRP Ann 67 (2018) 353–356.
[35] N. Liu, K. Sugawara, N. Yoshitaka, H. Yamada, D. Takeuchi, Damage-free highly efficient plasma-assisted polishing of a 20 mm square large mosaic single crystal diamond substrate, Sci. Rep. (2020) 1–7.
[36] P. Rupper, M. Amberg, D. Hegemann, M. Heuberger, Optimization of mica

surface hydroxylation in water vapor plasma monitored by optical emission spectroscopy, Appl. Surf. Sci. 509 (2020) 145362.
[37] Z. Fang, Y. Zhang, R. Li, Y. Liang, H. Deng, An efficient approach for atomic-scale polishing of single-crystal silicon via plasma-based atom-selective etching, Int. J. Mach. Tool Manufact. 159 (2020) 103649.
[38] J. Deng, L. He, B. Zhao, Q. Chen, Effects of air relative humidity on spectral characteristics of dielectric barrier discharge plasma assisted combustion reactor, Vacuum 175 (2020) 109189.
[39] K.A.M. Aboua, N. Umehara, H. Kousaka, T. Tokoroyama, M. Murashima, M.M. Bin Mustafa, et al., Effect of mating material and graphitization on wear of a-C:H coating in boundary base oil lubrication, Tribol. Lett. 68 (2020) 1–8.
[40] M. Varga, T. Izak, V. Vretenar, H. Kozak, J. Holovsky, A. Artemenko, et al., Diamond/carbon nanotube composites: Raman, FTIR and XPS spectroscopic studies, Carbon 111 (2017) 54–61.
[41] K.M. O'Donnell, C. Byron, G. Moore, L. Thomsen, O. Warschkow, A. Teplyakov, et al., Dissociation of CH3-O as a driving force for methoxyacetophenone adsorption on Si(001), J. Phys. Chem. C 123 (2019) 22239–22249.
[42] X. Wallart, C.H. De Villeneuve, P. Allongue, Truly quantitative XPS characterization of organic monolayers on silicon: study of alkyl and alkoxy monolayers on H-Si(111), J. Am. Chem. Soc. 127 (2005) 7871–7878.
[43] S. Ferro, M. Dal Colle, A. De Battisti, Chemical surface characterization of electrochemically and thermally oxidized boron-doped diamond film electrodes, Carbon 43 (2005) 1191–1203.
[44] Š. Meškinis, A. Vasiliauskas, M. Andrulevičius1, D. Peckus, S. Tamulevičius, K. Viskontas, Diamond like carbon films containing Si: structure and nonlinear optical properties, Materials 13 (2020) 59–71.
[45] J.W. Ma, W.J. Lee, J.M. Bae, K.S. Jeong, S.H. Oh, J.H. Kim, et al., Carrier mobility enhancement of tensile strained Si and SiGe nanowires via surface defect engineering, Nano Lett. 15 (2015) 7204–7210.
[46] W.J. Zong, T. Sun, D. Li, K. Cheng, Y.C. Liang, XPS analysis of the groove wearing marks on flank face of diamond tool in nanometric cutting of silicon wafer, Int. J. Mach. Tool Manufact. 48 (2008) 1678–1687.
[47] Y. Zheng, H. Ye, R. Thornton, T. Knott, T.J. Ochalski, J. Wang, et al., Subsurface cleavage of diamond after high-speed three-dimensional dynamic friction polishing, Diam. Relat. Mater. 101 (2020) 107600.
[48] M.R. Ammar, N. Galy, J.N. Rouzaud, N. Toulhoat, C.E. Vaudey, P. Simon, et al., Characterizing various types of defects in nuclear graphite using Raman scattering: heat treatment, ion irradiation and polishing, Carbon 95 (2015) 364–373.
[49] A.C. Ferrari, J. Robertson, Raman spectroscopy of amorphous, nanostructured, diamond-like carbon, and nanodiamond, Philos. Trans. R. Soc. A Math. Phys. Eng. Sci. 362 (2004) 2477–2512.